Korean J. of Chem. Eng., 3(2) (1986) 177-185

CREEPING FLOWS IN RECTANGULAR CAVITIES WITH TRANSLATING TOP AND BOTTOM WALLS: NUMERICAL STUDY AND FLOW VISUALIZATION

Hwa Won RYU and Ho Nam CHANG* Dong Il LEE**

Department of Chemical Engineering, Korea Advanced Institute of Science and Technology, P.O Box 150 Chongryang, Seoul, Korea

**Department of Chemical Engineering, Chonnam National University, Kwangju 505, Korea

(*Received 13 August 1985 • accepted 28 March 1986*)

Abstract—The recirculating flow patterns in the creeping flow range of an incompressible fluid in rectangular cavities with translating top and bottom walls were obtained numerically and by visualization, then were compared with each other. The aspect ratio was put to be either one or two.

Approximate solutions were obtained for various boundary conditions by using the variational method. The streamlines near the sharp corners were compared with some analytical solutions and the region in which the analytical solutions can safely be applied was confirmed.

INTRODUCTION

The cavity problem with a translating top wall has been one of the classical problems studied by Burggraf [1], De Vahl Davis and Mallinson [2], and Pan and Acrivos [3]. It has often been used to evaluate and test a newly developed numerical scheme. On the other hand, the top and bottom wall translating cavities have not been received much attention. Weiss and Florsheim [4] obtained an approximate solution of the symmetric flow solution at a low Reynolds number with a variational approach to biharmonic equation. O'Brien [5] studied an unsteady symmetric flow induced by oscillating plates in the same direction. Jagadish [6] also solved numerically the symmetric flow problem for the cavities having the aspect ratio of 1.0 and 2.0 with the Reynolds numbers up to 1000 numerically. A similar cases can be found in natural convective heat transfer in cavities with side walls held at different, but uniform temperatures [7]. However, little attention has been paid to the effect of the translating directions and the magnitude of the movements on the recirculating vortices in a cavity.

In this study we want to investigate numerically and experimentally the streamlines and velocities in the cavities with translating top and bottom walls by changing the moving directions and speeds of the top and bottom walls, and aspect ratios in the absence of apparent flux through the cavity. For the numerical convenience the scope will be limited to a creeping flows in rectangular cavities with aspect ratios of one and two. The result of this study will shed light on the convectional influence on the mass transport through the pore membrane with a small aspect ratio.

*To whom all correspondence should be addressed.

GOVERNING EQUATIONS AND APPROXIMATE SOLUTIONS

The steady motion in a fluid-filled rectangular cavity driven by the top and bottom walls in a uniform translational motion can be described by the following equations:

$$\nabla^2\psi = -\omega \tag{1}$$

$$\frac{\partial}{\partial x}\left(\frac{\partial \psi}{\partial y}\omega\right) - \frac{\partial}{\partial y}\left(\frac{\partial \psi}{\partial x}\omega\right) = \mathrm{Re}^{-1}\nabla^2\omega \tag{2}$$

where ψ and ω are the dimensionless stream function and vorticity respectively and Re is the Reynolds number. The variables have been scaled with the horizontal length of the cavity and the velocity of the sliding top wall as scale factors. The relations of stream function and vorticity to velocities are

$$u = \frac{\partial \psi}{\partial y}, \quad v = -\frac{\partial \psi}{\partial x} \tag{3}$$

$$\omega = \frac{\partial v}{\partial x} - \frac{\partial u}{\partial y} \tag{4}$$

The boundary conditions are

$$\psi=0,\quad \psi_x=0,\quad \text{at}\quad x=0 \tag{5}$$

$$\psi=0,\quad \psi_x=0,\quad \text{at}\quad x=1 \tag{6}$$

$$\psi=0,\quad \psi_y=u_B,\quad \text{at}\quad y=0 \tag{7}$$

$$\psi=0,\quad \psi_y=1,\quad \text{at}\quad y=H \tag{8}$$

where H is the dimensionless height of the cavity (Fig. 1). The horizontal velocity of the top wall is fixed to 1, while the horizontal velocity of the bottom wall, u_B, is varied to 2, 1, 0, -1 and -2. The aspect ratio (A.R.) or H is put to be either one or two.

A similar case is the creeping flow induced in a top-and-bottom-open cavity by a parallel shear flow through channels. To have approximate solutions sinusoidal velocity distributions are assumed both at top, y = H, and at bottom, y = 0. The maximum horizontal velocity at top is put to be one, while the maximum horizontal velocity at bottom (u_m) is varied from one to two. The direction of the flow at bottom is also varied. Variational method is used in the same manner as Weiss and Florsheim [4].

The boundary conditions used for the approximate solutions are Eqs. (5), (6) and the following ones:

$$\psi=0,\quad \psi_y=u_m\sin^2(\pi x)\quad \text{at}\quad y=0 \tag{9}$$

$$\psi=0,\quad \psi_y=\sin^2(\pi x)\quad \text{at}\quad y=H \tag{10}$$

The first order approximate solutions for $u_m = \pm 1$

$$\psi^{(1)}(x,y)=\frac{\pm\sin\beta(H-y)\sinh\alpha y-\sin\beta y\sinh\alpha(H-y)}{(\alpha\sin\beta H\mp\beta\sinh\alpha H)}\sin^2(\pi x) \tag{11}$$

and for $u_m = \pm 2$

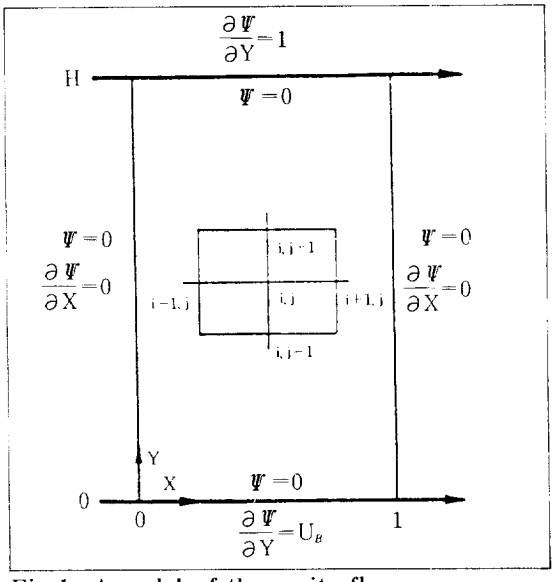

Fig. 1. A model of the cavity flow.

$$\psi^{(2)}(x,y)=\frac{(\pm2\alpha\sin\beta H+\beta\sinh\alpha H)\sin\beta(H-y)\sinh\alpha y-(\alpha\sin\beta H\pm2\beta\sinh\alpha H)\{\sinh\alpha(H-y)-\frac{\sinh\alpha(H+y)\}\sin\beta y}{(\alpha^2\sin^2\beta H-\beta^2\sinh^2\alpha H)}\sin^2(\pi x) \tag{12}$$

where

$$\alpha=\frac{2\pi}{3^{1/4}}\cos\frac{\theta}{2},\quad \beta=\frac{2\pi}{3^{1/4}}\sin\frac{\theta}{2},\quad \theta=\tan^{-1}\sqrt{2} \tag{13}$$

The velocities can be easily determined by substitution of the above results into Eq. (3).

NUMERICAL CALCULATION

To have a greater density of grids in the boundary layers adjacent to the walls, the governing equations are transformed with the following variables [7]:

$$\xi(x)=\frac{1}{2}\left[1-\tan\{(2x-1)\gamma\}/\tan\gamma\right] \tag{14}$$

$$\eta(y)=\frac{H}{2}\left[1+\tan\{(2y/H-1)\gamma\}/\tan\gamma\right] \tag{15}$$

Table 1 shows the non-equidistant grid points (21 × 41) in (x, y) coordinates when A.R. = 2, $\gamma=\pi/4$. The approximations of Eqs. (1) and (2) through the centered space difference yield

$$\psi=\frac{h^2\omega+\xi_x(\xi_x|_{i+1/2}\psi_{i+1}+\xi_x|_{i-1/2}\psi_{i-1})+\xi_x(\xi_x|_{i+1/2}+\xi_x|_{i-1/2})+\frac{\eta_y(\eta_y|_{j+1/2}\psi_{j+1}+\eta_y|_{j-1/2}\psi_{j-1})}{\eta_y(\eta_y|_{j+1/2}+\eta_y|_{j-1/2})}}{} \tag{16}$$

$$\frac{\mathrm{Re}}{4}\xi_x\eta_y[-\{\omega(\psi_{i+1}-\psi_{i-1})\}_{i+1}+\{\omega(\psi_{i+1}-\psi_{i-1})\}_{i-1}+\{\omega(\psi_{i-1}-\psi_{i-1})\}_{j+1}-\{\omega(\psi_{i-1}-\psi_{i-1})\}_{j-1}]+\xi_x\{(\xi_x)_{i+1/2}\omega_{i-1}+(\xi_x)_{i-1/2}\omega_{i-1}\}$$

Table 1. Grid points (A. R. = 2: $\gamma=\pi/4$).

x	0.0	0.034	0.070	0.111	0.156	0.205	0.258
	0.314	0.374	0.437	0.500	0.563	0.626	0.686
	0.742	0.795	0.844	0.889	0.930	0.967	1.0
y	0.0	0.033	0.067	0.103	0.141	0.181	0.222
	0.266	0.312	0.360	0.410	0.462	0.516	0.571
	0.629	0.688	0.749	0.810	0.873	0.936	1.0
	1.064	1.127	1.190	1.251	1.312	1.371	1.429
	1.484	1.538	1.590	1.640	1.688	1.734	1.778
	1.819	1.859	1.897	1.933	1.967	2.0	

$$\omega = \frac{+\eta_y\{(\eta_y)_{j-1/2}\omega_{j+1} + (\eta_y)_{j-1/2}\omega_{j-1}\}}{\xi_x(\xi_x|_{i+1/2} + \xi_x|_{i-1/2}) + \eta_y(\eta_y|_{j+1/2} + \eta_y|_{j-1/2})} \quad (17)$$

Grid speacing of $h = \Delta\xi = \Delta\eta = 1/20$ have been used here.

The SOR (successive over-relaxation) method is well applied to the above equations. The relaxation parameters for the calculation of both ϕ and ω are in the range of 1.2—1.6. The convergence criterion is defined as follows:

$$\sum_{\substack{i=0,n \\ j=0,n}} |f_{i,j}^{k} - f_{i,j}^{k-1}| < \varepsilon \quad (18)$$

where

$$\varepsilon = 1.0 \times 10^{-4} \sim 10^{-5}$$

EXPERIMENTAL

A schematic representation of the experimental apparatus for visualization is shown in Fig. 2. The outside wall of the box was made of 0.01 m thickness acryl plate; four brass wheels, two belts and a cavity were placed in it. The cavity of the size of $0.06 \times 0.06 \times 0.022$m (A.R. = 1) was used taking it into account that Mills [8] had a satisfactory results in a cavity with a span of 0.025m. After kneaded aluminium powder was plastered in the cavity wall, the cavity was fixed to the one of the walls of the box. Diluted glycerine (viscosity = 0.174 Pa·s, density = 1250 kg/m^3) was filled fully to the top of the box. A photographic film (0.035m) was used as belts and the wheels were toothed to fit the holes in the belts. Tensions of the belts were controlled with adjustment of the calibration knobs. Moving belts applied shear stresses to the liquid in the cavity, which subsequently made the liquid move. The speeds and the directions of the belts were controlled by D.C. motors which were connected to the axes of the bottom walls. The photographic system consisted of two 60 W electric lamp, a camera (Nikon FMII, Japan) with close-up lenses (King CU + 1, + 2 and + 4, Japan), and Kodak film (ASA 125).

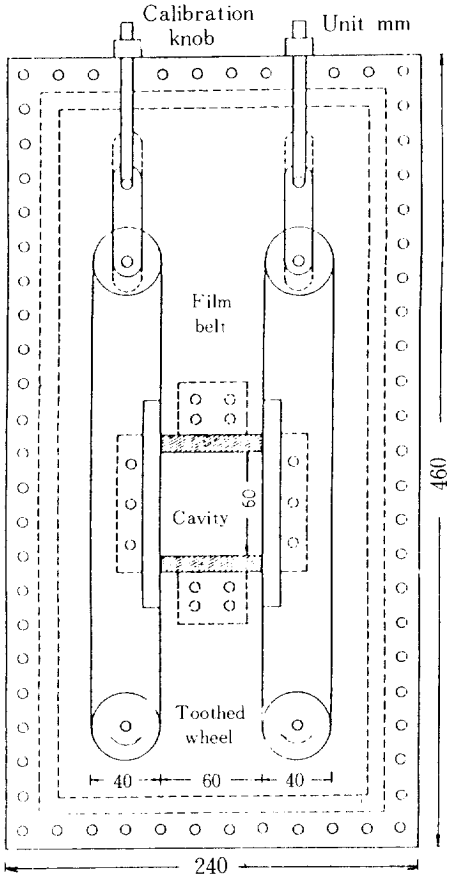

Fig. 2. Experimental apparatus.

RESULTS AND DISCUSSION

Flow Pattern for A.R. = 1

The calculated streamlines for A.R. = 1 are shown in Fig. 3. The streamlines at Re = 0.001 are symmetrical with respect to the vertical midplane of the cavity, x = 1/2. We cannot observe the inertial effects in the figure. The calculated streamlines at the same Re of the visualization experiment do not shift much from those at Re = 0.001 because the visualization experiments have been executed under the low Re range of 6—20.

When $u_B = 1$, eddies (or vortices) are formed in an even number and the flows are symmetrical with respect to y = H/2, the horizontal mid-plane. There exists a maximum in each vortex (Fig. 3(b)) and no flow occurs across the horizontal mid-plane. The case seems similar to a typical cavity problem with A.R. = 1/2 [3], except that the horizontal velocity at y = H/2 is not zero in spite $\phi = 0$ on it as will be seen in Fig. 5(a).

When u_B is increased from 1 to 2, the lower vortex expands wider and the upper vortex shrinks (Fig. 3(a)). One can also find that the stream function at the upper vortex center decreases while that the stream function at the lower one increases about twofold, from 0.0878 to 0.184. Considering that the maximum of the stream function is a measure of the strength of the vortex [2], it is interesting to note that the strength of the upper vortex is weakened by the expanded boundary of the lower vortex.

When $u_B = -1$, there exists one vortex with two maxima (Fig. 3(c)). The directions of the vortex is only one. The maximum stream function at the vortex is -0.120 which is higher than when $u_B = 1$. In the present case

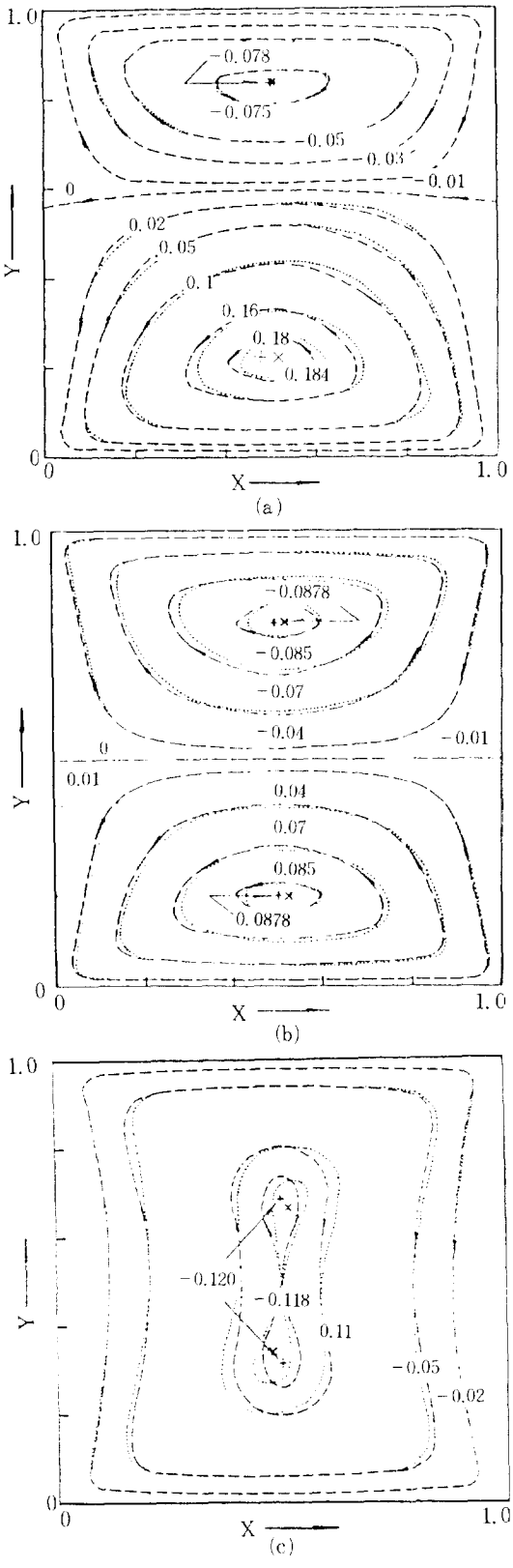

Fig. 3. Calculated streamlines for A. R. = 1, (⋯, + : Re = 0.001, ⋯, × : Re at Exp., Table 2).
(a) $u_B = 2$; (b) $u_B = 1$; (c) $u_B = -1$;
(d) $u_B = -2$; (e) $u_B = 0$

the mass or heat transfer between the top and the bottom wall is expected to be enhanced more than the case with $u_B = 1$ because the convective flow rotates all over the cavity.

When the magnitude of u_B is changed from -1 to -2, the two maxima become one and the vortex center moves downward (Fig. 3(d)).

When $u_B = 0$, secondary eddies at the right and left corners of the bottom wall are detected even with our 21 × 21 meshes by the coordinate transformation (Fig. 3(e)).

Fig. 4(a) shows the horizontal velocity profiles on the

vertical centerline of the cavity, x = 1/2, for A.R. = 1. The point at which u = 0 corresponds to the vortex center or saddle point. It is interesting to note that all the curves intersect each other at y = 0.24. The horizontal velocity at this point is about u = -0.11 in all cases, despite that the rotational directions and velocities of the lower vortices are different. When $u_B > 0$, the intersecting point lies above the primary eddy center nearest to the bottom wall and when $u_B < 0$, the converse is true.

Flow Pattern for A.R. = 2

Fig. 5 shows the streamline patterns for A.R. = 2. By comparing Figs. 5(a) and 5(b) to Figs. 3(a) and 3(b), we find that the effect of the velocity at bottom wall on the streamline is reduced as the aspect ratio increases. By increasing u_B from 1 to 2, the stream function at the bottom vortex center become approximately doubled, but the boundary between the vortices at the vertical midplane moves upward from y = 1.0 to only y = 1.06. When the direction of the moving walls are opposite, a saddle point is found at or near the cavity center in the contours of the stream function (Figs. 5(c) and 5(d)). The point has local maximum value of the absolute stream function in vertical direction and has local minimum value in horizontal direction. There are two eddy centers with opposite rotating directions. As u_B is changed from -1 to -2, the locations of the vortex centers are not much affected, the saddle point moves from y = 1.0 to 1.07, and the flow patterns are quite similar to each other. The horizontal velocity profiles on the vertical centerplane is shown in Fig. 4(b). The curves also intersect each other at y = 0.25 with the horizontal velocity of u = 0, approximately. The point is not expected to change much even if A.R. was higher than 2 for the point corresponds to the primary eddy center which is

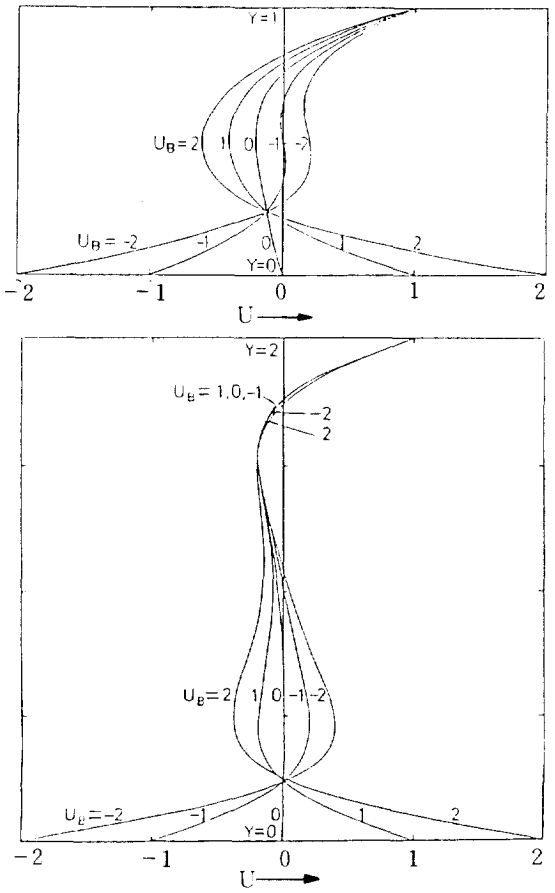

Fig. 4. U velocity profiles across the vertical center-planes at Re=0.001: (a) A.R. = 1; (b) A.R. = 2.

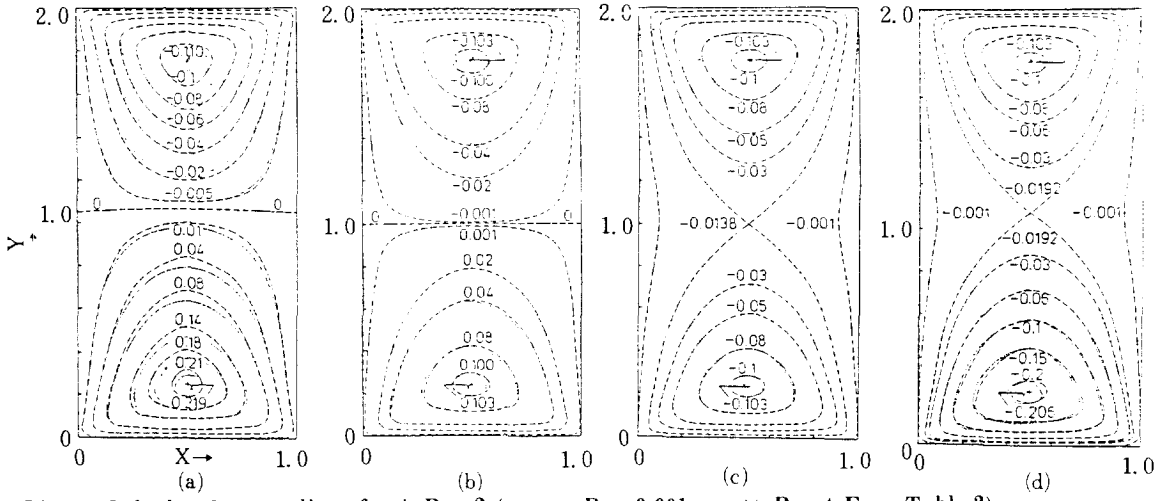

Fig. 5. Calculated streamlines for A.R. = 2, (···, —:Re=0.001, ····, ×:Re at Exp., Table 2).
(a) u_B=2; (b) u_B=1; (c) u_B=-1; (d) u_B=-2

known to be independent of A.R. when A.R. ≥ 2 [3].

Flow Pattern by the Approximate Solution

It has been found that the approximate solutions, Eq. (11) and Eq. (12), coincide well with the numerical solutions both at A.R. = 1 and at A.R. = 2. A typical streamlines of approximate solutions are compared with those of numerical ones in Fig. 6 when A.R. = 2 and $u_B = -1$. The eddy centers coincide with each other, although the patterns of the streamlines or the maximum value of the stream function at the eddy centers show a little differences. The positions of the vortex centers are (0.50, 0.30), (0.50, 0.70) at A.R. = 1 and (0.50, 0.22), (0.50, 1.78), at A.R. = 2, which are nearly the same as the results of the numerical solutions shown in Table 2. But the strength of the circulations are weak: the maximum stream function at the vortex centers are -0.0952 at A.R. = 1 and -0.0829 at A.R. = 2, respectively. The differences may be due to the inaccuracy of the solution or

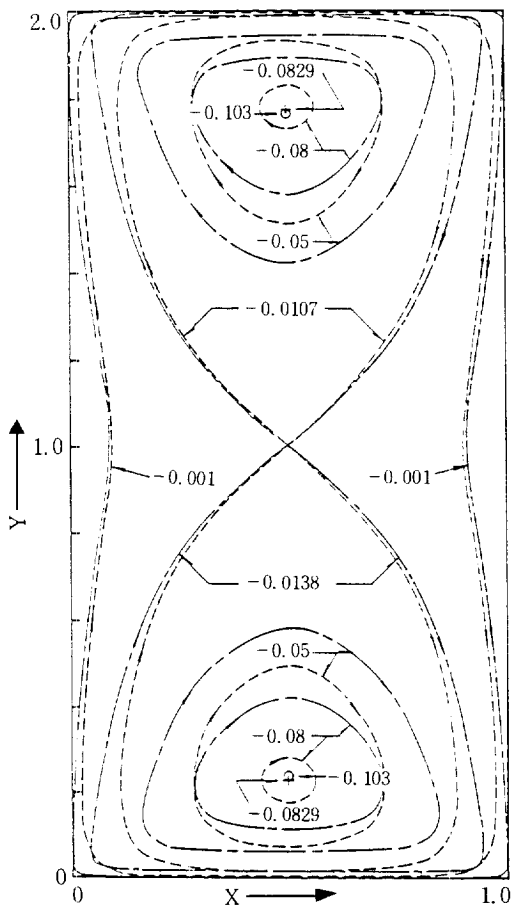

Fig. 6. Comparison of streamlines between numerical(— — —, ○) and approximate(···, +) solutions for A. R. = 2, $u_B = -1$.

to the fact that the mean velocity of the flow is low. The mean horizontal velocity of the fluid which applies shear forces at top of the cavity is

$$u_{mean} = \int_0^1 \sin^2 \pi x \, dx = 0.5 \tag{19}$$

One can find that it is only a half of the velocity at top wall for the numerical solution. The reason why the value of the stream function from approximate solution is so low may be attributed mainly to this fact. Nevertheless, it is still noticible that the vortex centers coincide well with each other in spite of the different boundary conditions.

Streamlines Near the Corners

It is an interesting thing to investigate how far the velocity of the bottom wall will influence the streamlines in the corners. Two cases are considered.

The first one is the upper corner where the vertical wall is stationary, while the horizontal wall is sliding over it with the velocity u = 1. The analytical solution of Moffat [9] is considered because the streamlines in the region very close to the upper corner is expected to be independent of the other walls which are far away from the corner. Moffat's solution can be modified as follows for the fitness of the coordinate system used here.

$$\psi = \{-\frac{\pi^2}{4}(H-y) + (\tan^{-1}(\frac{H-y}{x})) \left(\frac{\pi}{2}(H-y)+x\right)\} / \left(1-\frac{\pi^2}{4}\right) \tag{20}$$

At A.R. = 2, the streamlines are found to be independent of the bottom walls within radius of 0.2 when the corner point is taken as the origin; the influence of the direction or the velocity of the bottom wall on the streamlines in this region is negligible, as can be seen in Fig. 7(a). The figure also shows that Moffat's solution is successful to predict the stream function in it.

At A.R = 1, Fig. 7(b) shows that the streamlines near the moving plane are unaffected by the movement of the bottom wall up to the depth of about 0.08 from the upper plane. But the streamlines show more differences upon u_B as one goes from the stationary wall to the vertical center-plane of the cavity.

The second one is the corner formed by the vertical stationary wall and the horizontal center-plane moving toward the vertical wall in a right angle. The situation occurs when the upper and bottom walls move in the same direction with the same velocity. The horizontal velocity gradient with y is zero at the horizontal center-plane because of the symmetry about this plane. The problem is very similar to the two-dimensional flow near a point of zero friction described by Batchelor [10]. The following equation can be applied to the stream function at the lower left corner of the upper half plane of the cavity (Fig. 3(b), Fig. 5(b)).

Table 2. Position of vortex centers and boundary centers.

A. R.	u_B	Re. Exp.	Vortex center			Boundary center or saddle point		
			Experimental	Calculated		Experimental	Calculated	
				$Re=10^{-3}$	$Re=Exp.$		$Re=10^{-3}$	$Re=Exp.$
1	2	11.5	(0.50, 0.16) (0.50, 0.85)	(0.50, 0.21) (0.50, 0.83)	(0.53, 0.21) (0.51, 0.83)	(0.50, 0.59)	(0.50, 0.60)	(0.50, 0.60)
	1	17.5	(0.50, 0.16) (0.50, 0.84)	(0.50, 0.20) (0.50, 0.80)	(0.52, 0.20) (0.52, 0.80)	(0.50, 0.50)	(0.50, 0.50)	(0.50, 0.50)
	−1	19.8	(0.50, 0.20) (0.50, 0.80)	(0.50, 0.31) *(0.50, 0.30) (0.50, 0.69) *(0.50, 0.70)	(0.48, 0.35) (0.52, 0.65)	(0.50, 0.50)	(0.50, 0.50)	(0.50, 0.50)
	−2	11.5	(0.50, 0.75) (0.50, 0.21)	(0.50, 0.26)	(0.47, 0.26)	(0.50, 0.60)	–	–
2	2	6.3	(0.50, 0.24) (0.50, 1.76)	(0.50, 0.24) (0.50, 1.76)	(0.52, 0.23) (0.52, 1.77)	(0.50, 1.08)	(0.50, 1.06)	(0.50, 1.06)
	1	8.6	(0.50, 0.24) (0.50, 1.76)	(0.50, 0.24) (0.50, 1.76)	(0.51, 0.23) (0.51, 1.77)	(0.50, 1.0)	(0.50, 1.0)	(0.50, 1.0)
	−1	11.1	(0.50, 0.24) (0.50, 1.76)	(0.50, 0.24) *(0.50, 0.22) (0.50, 1.76) *(0.50, 1.78)	(0.48, 0.24) (0.51, 1.77)	(0.50, 1.0)	(0.50, 1.0)	(0.50, 1.0)
	−2	6.9	(0.50, 0.24) (0.50, 1.76)	(0.50, 0.24) (0.50, 1.76)	(0.48, 0.23) (0.51, 1.77)	(0.50, 1.07)	(0.50, 1.07)	(0.50, 1.07)

*The values are from the approximate solution.

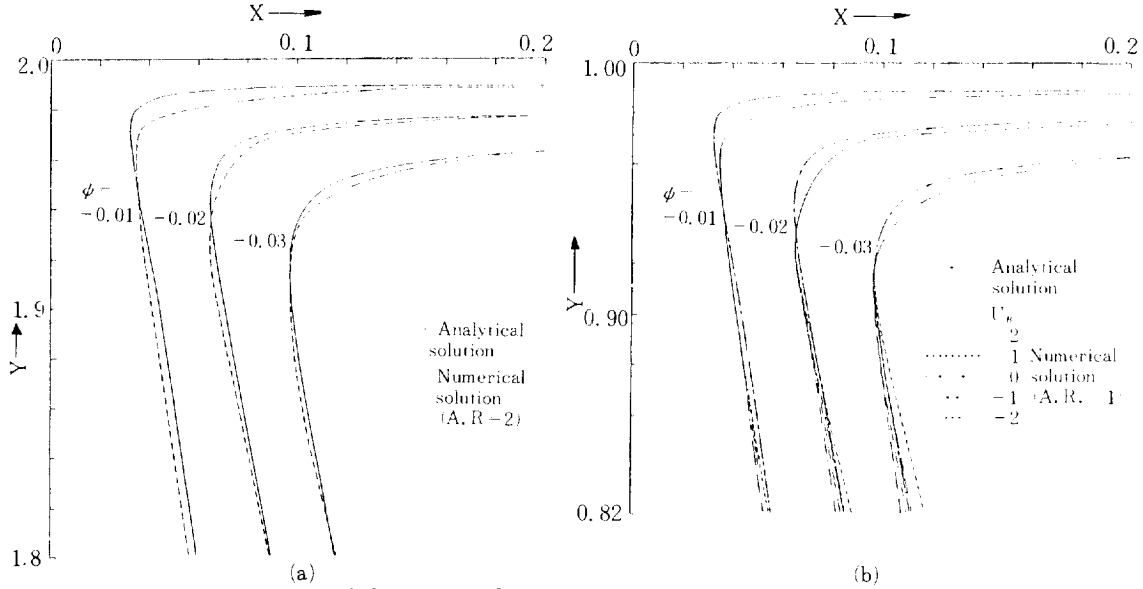

Fig. 7. Streamlines near upper left corner of the cavity.
(a) A. R. =2, (b) A. R. =1

$$\psi = Ax(y - H/2)^2 \quad (21)$$

where A means an arbitrary constant and we put A = 10. Because of the arbitrariness of A, direct comparison of the values of the stream function from analytical solution with those from the numerical solution is meaningless; Fig. 8 is provided only to compare the flow patterns of these two cases. It is found that the turning angle of the streamlines from the analytical solution are a little larger than those from the numerical calculation. There is little dependence of the patterns of the streamlines upon aspect ratios. However, values of the stream function near the corner at A.R. = 2 is weaker than those at A.R. = 1 in the order of 10.

Flow Visualization

Fig. 9 and Fig. 10 show photographs of steady-state flow patterns for A.R. = 1 and A.R. = 2. The Reynolds number based on the velocities of the top wall are in the range of 6.3—19.8 owing to the difficulty of the visualization in the creeping flow region. Thus flow patterns shown in Figs. 9 and 10 do not reflect those of creeping flow regions in a true sense. However, the symmetrices observed with respect to the vertical midplanes resemble those of creeping flow regions. Thus we assume that the recirculating flows in the creeping flow range are similar to those observed here but perhaps with reduced strength. Table 2 compares the theoretical predictions at the experimental conditions and those at the creeping flows. The y-positions of the vortex center are in good agreement with each other, however, x-positions of the experimental conditions

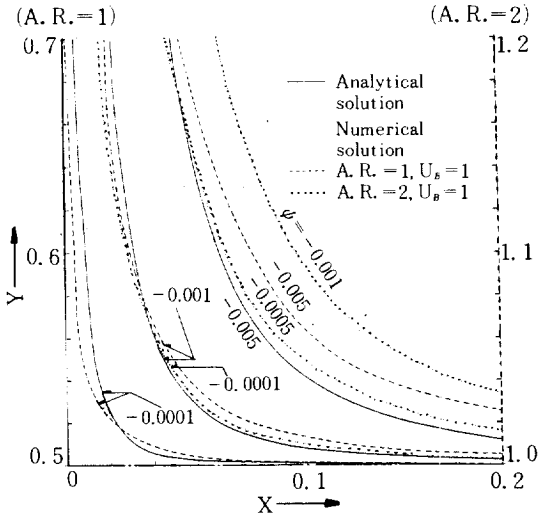

Fig. 8. Streamlines in a corner between vertical wall and horizontal center-plane of the cavity.

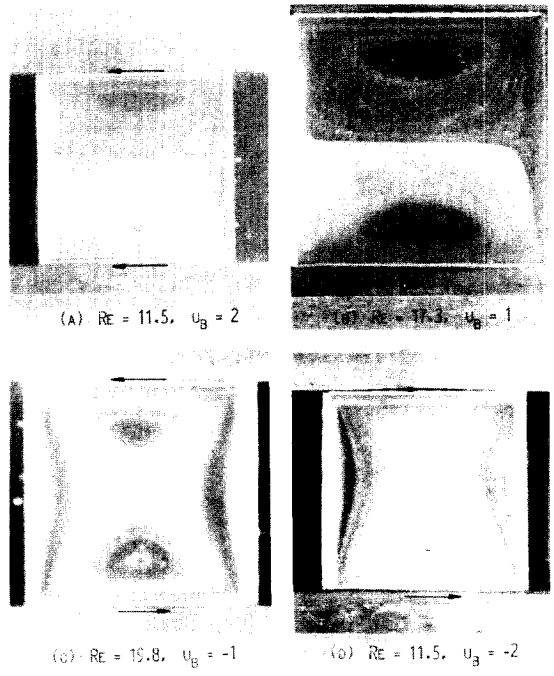

Fig. 9. Photographs of flow patterns for A.R.=1.
(a) Re=11.5, u_B=2 (b) Re=17.3, u_B=1
(c) Re=19.8, u_B=−1 (d) Re=11.5, u_B=−2

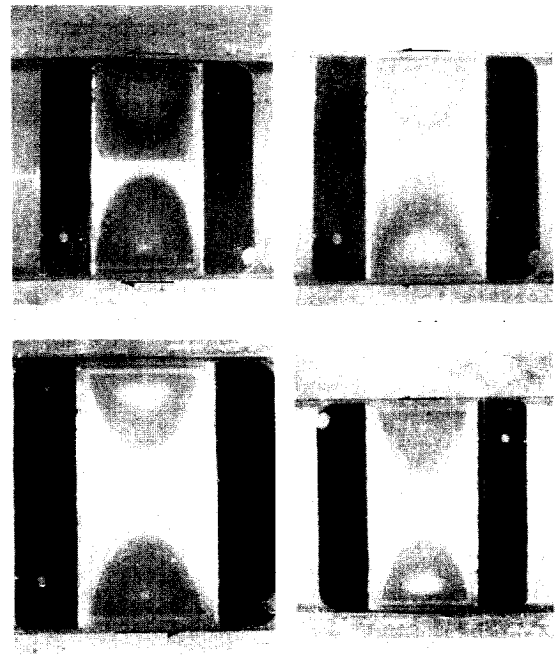

Fig. 10. Photographs of flow patterns for A.R. =2.
(a) Re=6.3, u_B=2 (b) Re=8.6, u_B=1
(c) Re=11.1, u_B=−1 (d) Re=6.9, u_B=−2

in higher Re are slightly shifted from 0.5 of the creeping flows. Moreover, Table 2 shows the comparison of the vortex centers and saddle points from experiments with those from calculations. The results seem to be successful except when A.R. = 1, $u_B < 0$. When u_B has a negative value the flow in cavity is thought to be hydrodynamically unstable due to the inflection point [11] as is shown in Fig. 4(a) and 4(b). But it is not clear whether this discrepancy is due to the 3-dimensional effect or to the unstableness with experimental error. More investigations are required to clarify this.

When A.R. = 1 and $u_B = 1$ or 2, Figs. 9(a) and 9(b) show the vortex boundaries or flow patterns are much alike to the theoretical solutions shown in Figs. 3(a) and 3(b). No convective flow is observed through this vortex boundary. When $u_B = 2$, the experimentally found y-postion of the boundary center between the vortices is 0.59, which is well compared to 0.60 by the theory. The vortex centers, however, shifted a little upward comparing to the theoretical results.

When $u_B = -1$, the property of centro-symmetry is preserved and the outer streaklines are exactly the same as the predicted one (Fig. 9(c)). But the generated vortex centers locate at y = 0.20 and 0.80 and deviate from the theoretical results of y = 0.31 or 0.35, and 0.69 or 0.65.

As u_B is changed to −2, the upper vortex shrinks. It does not disappear completely (Fig. 9(d)), a small weak vortex is still observed. On the whole, however, the flow pattern agrees well with the calculated one; the convective flow sweeps all over the cavity actively

Fig. 10 shows photographs of the flow patterns for A.R. = 2. Suprisingly, the visualization results are well in accord with the theoretical predictions. The barrier between the two vortices are sharply seen in Figs. 10(a) and 10(b). Also the saddle points are clearly observed at the center of the cavity in Figs. 10(c) and 10(d).

CONCLUSIONS

The following conclusions have been obtained under the conditions of A.R. = 1 and 2, $Re < 20$ and $-2 \leqq u_B \leqq 2$.

1. When $u_B > 0$, the eddies are formed in an even number and there is no convective flow through the boundary between the eddies.
2. When $u_B < 0$, the mass or heat transfer between the top and bottom walls is expected to be enhanced because of the convective flow rotating all over the cavity.
3. There exists a point at which the magnitudes of u on vertical centerplane of the cavity are in accord with each other. When A.R = 1, y = 0.24 corresponds to that point with a value of u = −0.11 and when A.R. = 2, y = 0.25 does with u = 0.
4. The Moffat's and Batchelor's analytical solution describe well the streamlines of the eddies near the corners.
5. The flow patterns from visualization experiment is predicted well by the present numerical solution except when A.R. = 1, $u_B < 0$.

NOMENCLATURE

A.R.	:	aspect ratio (–)
f	:	vorticity or stream function (–)
H	:	height of a cavity (–)
h	:	mesh size (–)
L	:	width of a cavity (m)
m, n	:	number of divisions in x-, y- directions (–)
Re	:	Reynolds number, Lu_T/ν(–)
u	:	x-direction velocity (–)
u_B	:	x-direction velocity of the bottom wall (–)
u_m	:	maximum x-direction velocity at bottom in a boundary condition for the approximate solution (–)
u_T	:	x-direction velocity of the top wall (m/s)
v	:	y-direction velocity (–)
x, y	:	x-, y-coordinates (–)
γ	:	deformation parameter (–)
ε	:	convergence criterion (–)
ν	:	kinematic viscosity (m^2/s)
ξ, η	:	transformation relation (–)
ξ_x, η_y	:	$\frac{\partial \xi}{\partial x}, \frac{\partial \eta}{\partial y}$ (–)
ψ	:	stream function (–)
ω	:	vorticity (–)
∇	:	del operator (–)

REFERENCES

1. Burggraf, O.R.: *J. Fluid Mech.*, **24,** 113 (1966).
2. De Vahl Davis, G. and Mallinson, G.D.: *Computers and Fluids*, **4,** 29 (1976).
3. Pan, F. and Acrivos, A.: *J. Fluid Mech.*, **110,** 433 (1981).
4. Weiss, R.F. and Florsheim, B.F.: *Phys. Fluids*, **8,** 1631 (1965).
5. O'Brien, V.: *AIAA J.* **13,** 415 (1975).
6. Jagadish, B.S.: *J. Fluids Eng.*, **99,** 526 (1977).
7. Kublbeck, K., Merker, G.P. and Straub, J.: *Int. J. Heat Mass Transfer*, **23,** 203 (1980).
8. Mills, R.D.: *J. Roy. Aero. Soc.*, **69,** 714 (1965).
9. Moffat, H.K.: *J. Fluid Mech.*, **18,** 1 (1964).
10. Batchelor, G.K.: "An Introduction to Fluid Dynamics", Cambridge Univ. Press, London, Great Britain (1967).
11. Schlichting, H.: "Boundary Layer Theory", 7th ed., McGraw-Hill, New York, NY(1979).